ACS OMEGA

http://pubs.acs.org/journal/acsodf

Article

Effect of Elevated Temperature on the Microstructure of Metakaolin-Based Geopolymer

Stephen Adjei, Salaheldin Elkatatny,* and Korhan Ayranci

Cite This: *ACS Omega* 2022, 7, 10268−10276

Read Online

ACCESS | Metrics & More | Article Recommendations

ABSTRACT: Currently, geopolymer is being considered as a future oil-well cement. For wellbore applications, geopolymers are initially tested at specific temperature conditions. However, an oil-wellbore may experience a sudden increase in temperature which may adversely affect geopolymer systems designed for low to moderate temperature conditions. In this work, the effect of elevated temperatures on the microstructure of the geopolymer was simulated. Metakaolin-based geopolymer systems cured at 163 °F for 48 h were subjected to a temperature ramp of 194 °F and 248 °F for 24 h. X-ray diffraction, Fourier transform infrared spectroscopy, and thermogravimetry analysis techniques were used to study the microstructural changes. The analytical techniques show the formation of new crystalline phases when the geopolymer cured at 163 °F was suddenly exposed to higher temperatures. These crystalline phases, for instance, gobbinsite and anorthite, observed in the microstructure have the potential to cause thermal stress, weaken the system, and ultimately affect the geopolymer's ability to effectively isolate the formation and support the casing.

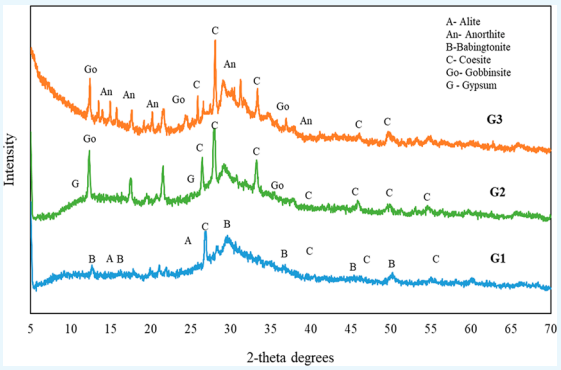

1. INTRODUCTION

The production of ordinary Portland cement (OPC) is one of the main sources of anthropogenic carbon dioxide (CO_2) output, contributing around 5−7%.[1,2] This necessitates the investigation of alternative cement systems with low CO_2 emissions.[3] Geopolymer is one of the most used alternative cementitious systems.[4,5] The geopolymer is a type of cementitious material (inorganic polymeric binder) formed when aluminosilicate-rich precursors are dissolved in alkaline solutions and undergo a polycondensation reaction.[5]

The application of geopolymer systems in oil-well cementing is still in the research stage. A review study by Adjei et al.[6] discussed the investigations that have been performed to date. These studies can be classified under four main categories: (1) geopolymer application in acidic and high saline environments,[7−13] (2) geopolymer application in well plug and abandonment,[14−17] (3) compatibility of geopolymer with drilling mud,[18−22] and (4) effect of temperature on geopolymer systems.[23−26] These studies indicated that in comparison to OPC systems, a geopolymer is more durable in aggressive environments, could be an excellent plug material, and is highly compatible with drilling fluid.

In the fourth category (effect of temperature), researchers developed geopolymer systems simulating fixed temperature conditions. It has been reported that the optimum performance of geopolymer systems can be achieved when they are generally cured at 122−176 °F.[27,28] Nasvi et al.[23] observed the optimum temperature within 122 °F to 140 °F. Nasvi et al.[24] explored the feasibility of geopolymer as a binder in oil and gas wells designated for carbon dioxide storage. The study indicated higher strength for a geopolymer system cured at 144 °F, however the authors reported that a slight increase in strength has been observed up to 185 °F. Nasvi et al.[25] also noticed that the carbon dioxide permeability increased with increasing curing temperature. Even though the increase was lower compared to the OPC-based system, such a scenario would decrease the sealing ability of the geopolymer.

The above findings have shown that geopolymer systems would be idle for low to moderate temperature conditions. However, cementitious systems placed in shallow intervals may be subjected to elevated temperatures during the hardening period. For instance, drilling, completions, and workover operations and production techniques such as cyclic steam injection may cause elevation of downhole temperature that would adversely impact the cement sheath.[29−31] In the case of conventional Portland cement systems, studies have shown that

Received: December 5, 2021
Accepted: March 1, 2022
Published: March 14, 2022

Table 1. Chemical and Physical Properties of Raw Materials

raw materials	SiO_2	Al_2O_3	Fe_2O_3	CaO	K_2O	Na_2O	MgO	SO_3	TiO_2	specific gravity
GGBFS	35.30	14.21	0.50	43.79	0.00	0.00	0.00	0.00	0.75	2.89
PKS	55.55	27.48	12.08	0.00	3.07	0.00	0.33	0.00	1.49	2.60

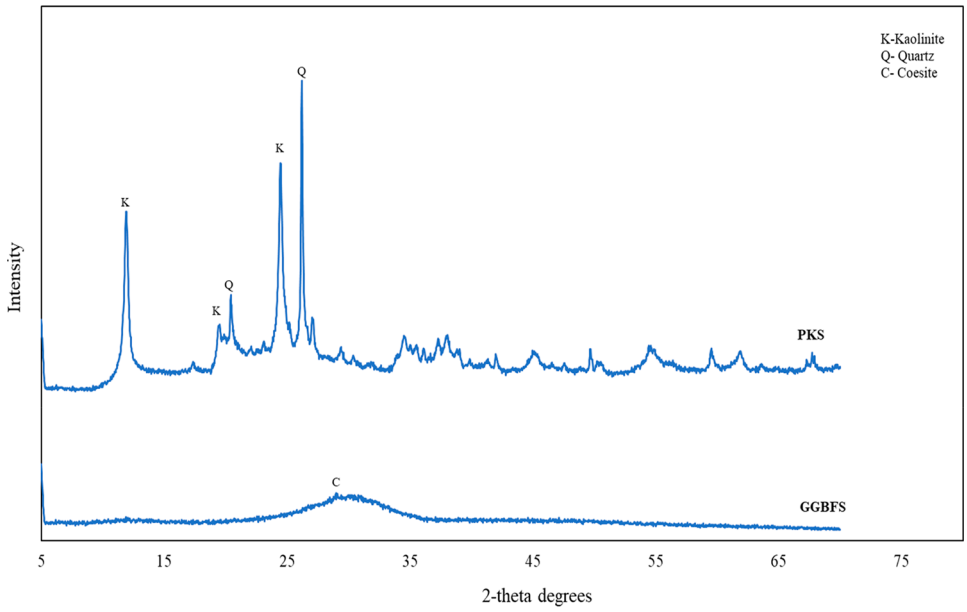

Figure 1. Diffractogram showing mineral phases present in powdered kaolinitic shale and ground granulated blast furnace slag.

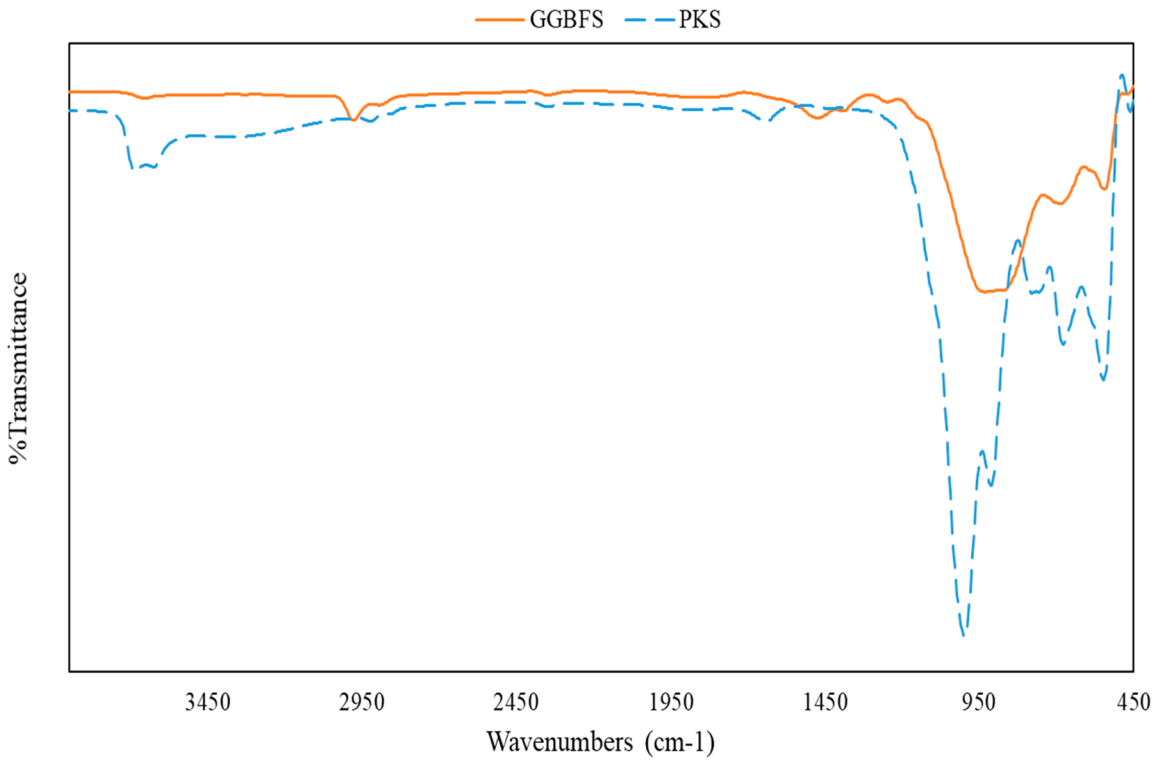

Figure 2. Infrared spectrum of powdered kaolinitic shale and ground granulated blast furnace slag.

above 230 °F, the calcium silicate hydrate gel produced through cement hydration is converted into a more dense phase known as alpha dicalcium silicate hydrate, which has a detrimental effect on the cement system.[32−35] The addition of a silica source modifies the C−S−H phase into more stable phases like tobermorite and Xonotlite.[34]

The macroscopic effect of elevated temperatures has been well documented. The objective of this current study is to understand the microstructural effect of elevated temperatures.

https://doi.org/10.1021/acsomega.1c06878
ACS Omega 2022, 7, 10268−10276

X-ray diffraction (XRD), Fourier transform infrared (FTIR) spectroscopy, and thermogravimetry analysis (TGA) were used to better understand the effect of sudden temperature increase on the geopolymerization process of the geopolymer developed using metakaolin produced locally from the calcination of Saudi kaolinitic shale.

2. MATERIALS AND METHOD

2.1. Materials. In this study, powdered kaolinitic shale (PKS) was converted into metakaolin for the synthesis of the geopolymer. The PKS was obtained by grinding mudrocks collected from the Qusaiba Member of Qalibah Formation, Saudi Arabia. Ground granulated blast furnace slag (GGBFS) was combined in the synthesis of the geopolymer. The chemical composition of the raw materials as indicated by the X-ray fluorescence (XRF) and the specific gravity of these materials is given in Table 1. Both PKS and GGBFS are dominated by silica and alumina, which are required in geopolymerization. A Bruker X-ray diffractometer (XRD) was used for characterizing the mineral phases within a scanning range of 5−70°, 2θ. The diffractogram (Figure 1) shows that the GGBFS is highly amorphous, showing a hump at 25−35°, 2θ°. The GGBFS also shows the presence of crystals of coesite (100%), a polymorph of crystalline silicon dioxide.[36] The PKS contains kaolinite (77%) and quartz (22.6%). A Nicolet FTIR device was used to collect spectra data within the 400−4000 cm^{-1} range. The infrared (IR) spectrum of the GGBFS and PKS is presented in Figure 2. The OH-stretching and Al−OH deformation bands of kaolinite appear at 3000−4000 and 912.51 cm^{-1}, respectively. The asymmetric Si−O−Si (Al) stretching vibration occurs at 998−1034 cm^{-1}. The Si−O-symmetrical stretching vibration of SiO_2 appears at 678−763 cm^{-1}.[37−39] The intensity of the bands in the OH-stretching region is not pronounced in the PKS, implying a low degree of orderliness, making it an excellent source for metakaolin production.[39]

The alkaline solution was a mixture of sodium hydroxide (NaOH) and sodium silicate (Na_2SiO_3). The NaOH having ≥98% purity was supplied by Sigma-Aldrich. The Na_2SiO_3 (SiO_2/Na_2O = 3.375, specific gravity = 1.390) was obtained from Loba Chemie, India. Distilled water was used in all the formulations.

2.2. Methodology. *2.2.1. Conversion of PKS to Metakaolin.* The PKS (75 μm) was placed in an oven at 1562 °F for 1 h to produce metakaolin.[40] Earlier investigations had revealed this to be the optimum calcination temperature for the kaolinitic shale used in this study. XRD, FTIR, and thermogravimetry analysis (TGA) were used to study the dehydroxylation process. The XRD and FTIR tests were performed using the same equipment and conditions as discussed earlier. The powders were also placed in an SDT Q600 device manufactured by TA Instruments and heated from the ambient room temperature up to about 1634 °F at a rate of 50 °F/min in an atmosphere of air.

2.2.2. Determination of Minimum Required Silicate Modulus. The initial objective was to determine the minimum silicate modulus (Ms) required to have an alkaline solution with suitable gelation. A modulus silicate of 0.7, 0.9, and 1.1 was initially investigated. The NaOH was used to adjust the silicate modulus. The NaOH pellets were dissolved in the sodium silicate solution and allowed to cool down to ambient room temperature. Distilled water was used to adjust the H_2O/Na_2O ratio of the silicate solution. The H_2O/Na_2O controls the alkalinity and workability of the slurry and it has been reported that a value of 11/12 gives the optimum workability.[41,42] In this work, an H_2O/Na_2O of 11 was used in all systems.

2.2.3. Geopolymer Synthesis. A binary geopolymer system was developed using the PKS and GGBFS in the ratio of 70:30 (PKS/GGBFS) by weight of blend (BWOB). The choice of GGBFS was based on the report by several authors that it enhances the setting and contributes to strength, especially at an optimal level of 30%.[13,43−45] The sodium bentonite was dry presheared at 12 000 rpm for 5 min. The PKS and GGBFS were added to the liquid phase composed of the alkaline solution, defoamer, and dispersant. The role of sodium bentonite was to control free water and sedimentation observed in the initial trial tests. The mixing of the slurry, conditioning, rheology, and thickening time tests were according to the guidelines provided by American Petroleum Institute (API).[46,47] The recipes for the geopolymer system are given in Table 2.

Table 2. Mix Design for Geopolymer

material	proportion, %BWOB
PKS	70
GGBFS	30
sodium bentonite	10
defoamer	0.3
alkaline solution/binder ratio	4

2.2.4. Curing. The slurries were poured into 1.5 in. × 4 in. cylindrical molds. The molds (three samples for each system) were placed in aging cells containing distilled water and then placed in an electric oven. A pressure of 200 psi was applied to the aging cells. The geopolymer systems were all initially cured at 163 °F for 48 h. Then the control sample (aged at 163 °F for 48 h) was taken out of the oven, and the temperature was ramped up to 194 °F and kept at this temperature for 24 h. The experiment was repeated for a temperature rise of 248 °F. Microstructural analyses were performed at the end of each curing period.

3. RESULTS AND DISCUSSION

3.1. Investigating the Conversion of PKS to Metakaolin. *3.1.1. XRD Analysis of Raw and Heated PKS.* The characterization of the PKS indicated the presence of kaolinite (K) in a high proportion (77%) (Figure 1). Such a high amount of kaolinite implies the rock can be categorized under high grade, a category that possesses the potential of being highly reactive upon heat treatment.[37,48] The diffractogram in Figure 3 shows that while the peak of quartz is present that of kaolinite disappears upon heat application. This is probably due to dehydroxylation of the structural water indicating the transformation of kaolinite into metakaolin, confirmed by the presence of a halo hump between 20 and 35°, 2θ.[49]

3.1.2. FTIR of Raw and Heated PKS. The FTIR can be used to study the dehydroxylation process by monitoring the behavior of the bands associated with the OH groups. When the OH groups in the clays' structure are removed, the material loses its crystal structure and becomes amorphous.[50] When a rock contains more than one clay mineral, it is sometimes difficult to characterize it using the FTIR technique due to overlap in the spectra. However, this sample shows only kaolinite, which makes the use of FTIR efficient. Figure 4 compares the IR spectrum before and after heat treatment. The two peaks in the 3000−4000 cm^{-1} range attributed to OH-stretching vanish upon heating, indicating dehydroxylation has taken place.[37,39]

https://doi.org/10.1021/acsomega.1c06878
ACS Omega 2022, 7, 10268−10276

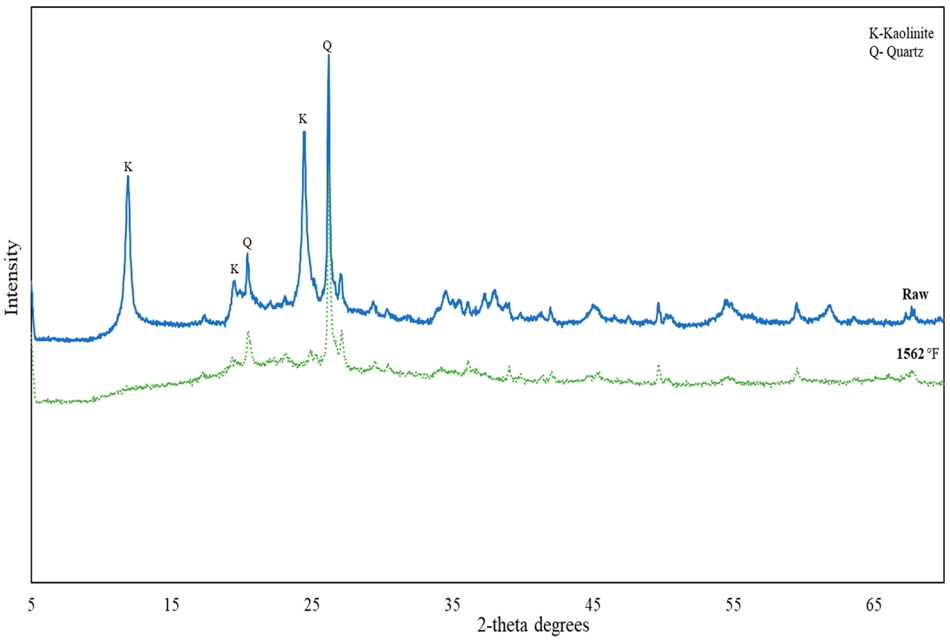

Figure 3. Diffractogram showing the effect of temperature on the powdered kaolinitic shale.

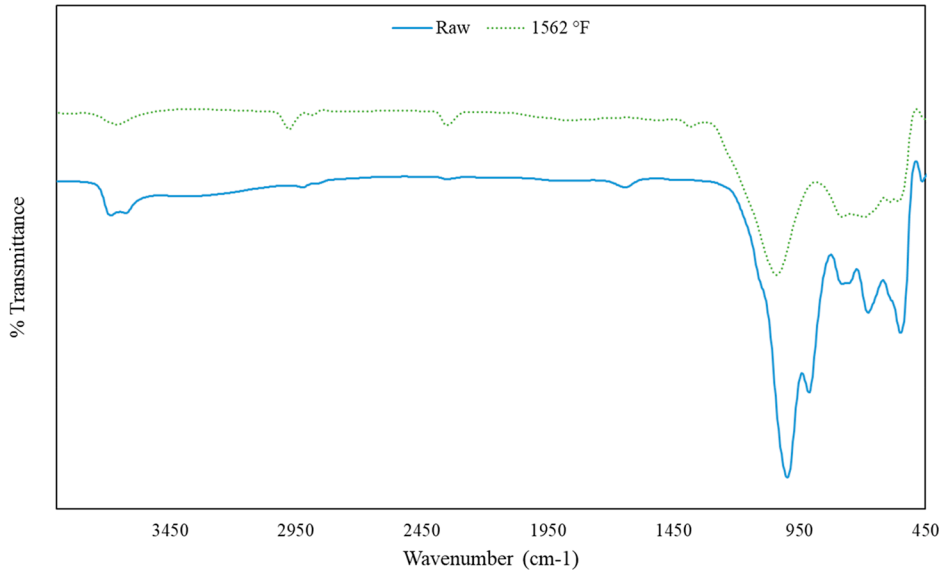

Figure 4. IR spectrum showing the effect of temperature on the powdered kaolinitic shale.

Dehydroxylation is further confirmed in the disappearance of the OH-deformation band at 912.51 cm^{-1} in the heated sample.[39,51] The change in the microstructure upon heating is also inferred from the intensity of the bands at 998−1037 cm^{-1} attributed to the asymmetric Si−O−Si (Al) stretching.[39,52]

3.1.3. Thermogravimetry Analysis of Raw and Heated PKS. Figure 5 compares the weight loss of the raw and heated samples. The loss of structural water at certain temperature intervals could be used to infer the dehydroxylation process. In the raw sample, the weight loss up to about 230 °F is due to the removal of the adsorbed water in the interlayer of the clay mineral while the loss between 959 °F and 1634 °F is due to dehydroxylation.[37,53,54] It is confirmed that the material undergoes dehydroxylation upon heat treatment, inferred from the negligible weight loss in the regions associated with the loss of structural water. The total weight loss in each of the samples is provided in Table 3.

3.2. Minimum Silicate Modulus. The silicate modulus (Ms) of the sodium silicate solution controls the extent of gepolymerization and hence affects parameters like setting, viscosity, and strength.[55−57] Commonly used ratios fall within the range of 0.6 to 2 with the authors reporting various optimum values.[57−62] It was necessary to determine the minimum Ms that would help to achieve a workable solution. Figure 6 compares the behavior of alkaline solutions with Ms of 0.7, 0.9, and 1.1. The system with a Ms of 0.7 (Figure 6a) quickly gels as the solution cooled down, however, when the Ms is increased to 0.9 the rate of gelling reduces. In Figure 6b, the solution is clear and remains in this state for about 4 h, however, precipitation begins in Figure 6c after about 4 h, and severe precipitation occurs in Figure 6d at 24 h. However, the solution designed at Ms of 1.1

https://doi.org/10.1021/acsomega.1c06878
ACS Omega 2022, 7, 10268−10276

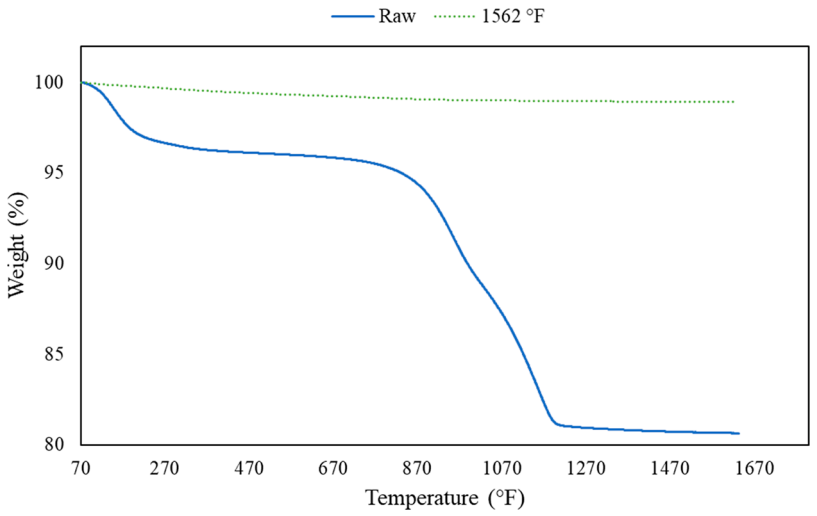

Figure 5. Thermogram of raw and heated powdered kaolinitic shale powders.

Table 3. Total Weight Loss of Samples at the End of the Test

sample	weight loss, %
raw	19.36
1562 °F	1.08

remains clear and stable for the entire 24 h period. The objective of this study is not to investigate the effect of Ms and hence the minimum Ms required to achieve a workable alkaline system, which in this investigation 1.1 was selected.

3.3. Rheology and Viscosity. The consistency plot (Figure 7) of the developed geopolymer was fitted with the Bingham plastic model (BP). The model fits the data with a coefficient of determination (R^2) of 99.9%. The slurry has a yield stress of about 1.06 lbf/100 ft^2. The plastic viscosity is approximately 0.178 lbf/100 ft^2 (85 cP). The plot of the shear rate versus viscosity plot in Figure 8 indicates that the developed system has a shear thinning behavior, which is the desired flow behavior for oil-well cementing. The above parameters show that the geopolymer system exhibits good flow behavior.

3.4. Thickening Time. Cement systems should have a reasonable setting or thickening time to allow for efficient cement placement. In conventional cement systems, the time a slurry achieves a consistency value of 70 or 100 Bearden unit of consistency (Bc) is often reported as the thickening time.[46] The consistency of the slurry at different times is shown in Figure 9. The investigation was done up to 70 Bc. The initial consistency of the slurry is about 4.8 Bc and it achieves 70 Bc in about 3 h and 26 min.

3.5. Results and Discussion. *3.5.1. XRD Analysis of Geopolymer Systems.* The mineralogical composition of the geopolymer systems aged under different temperature conditions is presented in Figure 10. All geopolymer systems show an equivalent amorphous hump at 20 to 40°, 2θ°. This indicates the formation of the aluminosilicate gel and amorphous calcium silicate hydrates from the geopolymerization of the metakaolin and GGBFS, respectively.[43,63,64] The control sample cured at 163 °F only, G1, shows the presence of alite, coesite, and babingtonite. The alite is from the dissolution of both raw materials. The coesite is from the GGBFS, while the babingtonite ($Ca_2(Fe,Mn)FeSi_5(OH)_{14}$) is associated with zeolite minerals.[65] When the temperature was ramped to 194 °F (G2), coesite, gobbinsite ($Na_5(Si_{11}Al_5)O_{32}\cdot 11H_2O$), and gypsum are seen in the microstructure while anorthite crystallizes at 248 °F (G3). The gobbinsite and anorthite (CaO, Al_2O_3, $2SiO_2$) are related to the zeolite group.[66−68] In general, the diffractogram shows an increase in crystallinity with increasing curing temperature. Increased crystallization could lead to thermal stress in the microstructure which would degrade the system.[69,70]

3.5.2. FTIR Analysis of Geopolymer Systems. The FTIR technique is accurate in determining tiny changes in the microstructure.[11] The significant difference in the infrared (IR) spectra (Figure 11) is a confirmation of the formation of new

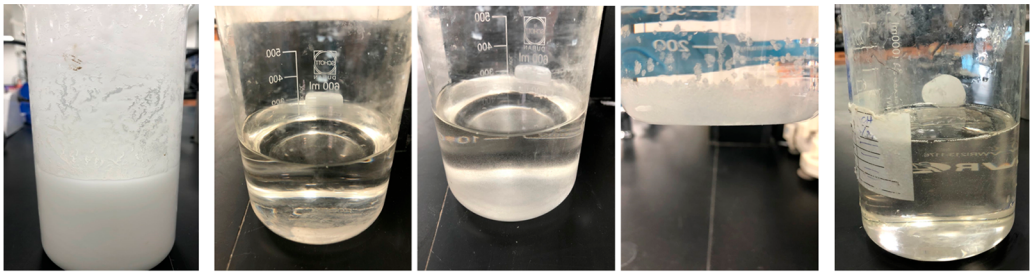

a. Ms= 0.7 b. M= 0.9 c. Ms= 0.9 d. Ms= 0.9 d. Ms =1.1

Figure 6. Effect of modulus silicate on the alkaline system.

https://doi.org/10.1021/acsomega.1c06878
ACS Omega 2022, 7, 10268−10276

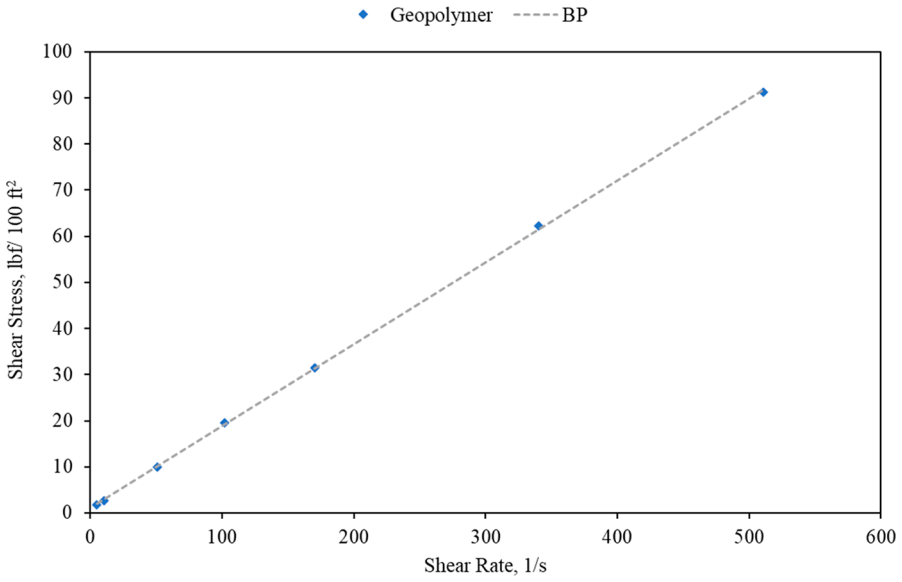

Figure 7. Rheology of metakaolin-based geopolymer at 114 °F.

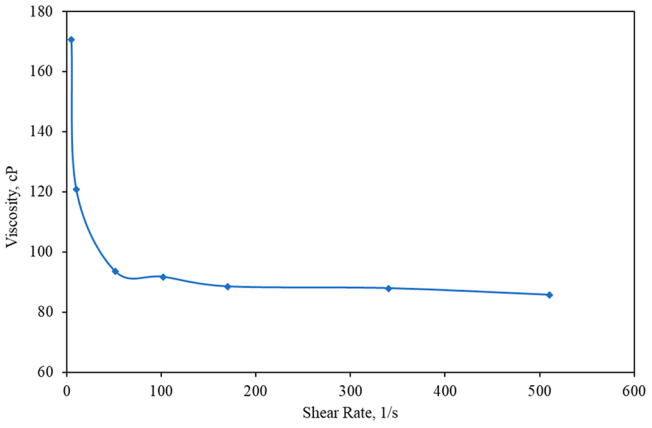

Figure 8. Viscosity of metakaolin-based geopolymer at 114 °F.

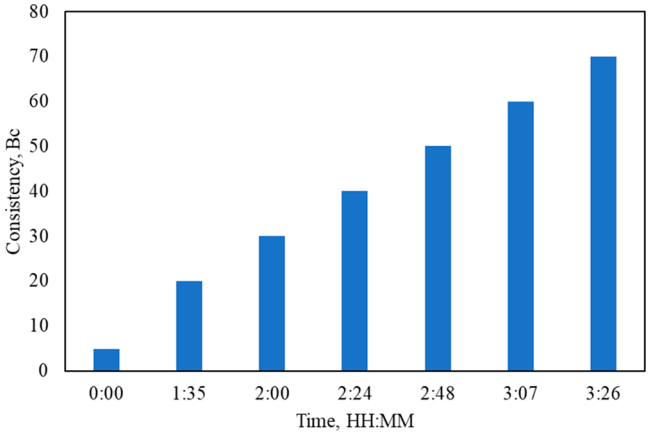

Figure 9. Thickening time of synthesized geopolymer system at 114 °F and atmospheric pressure.

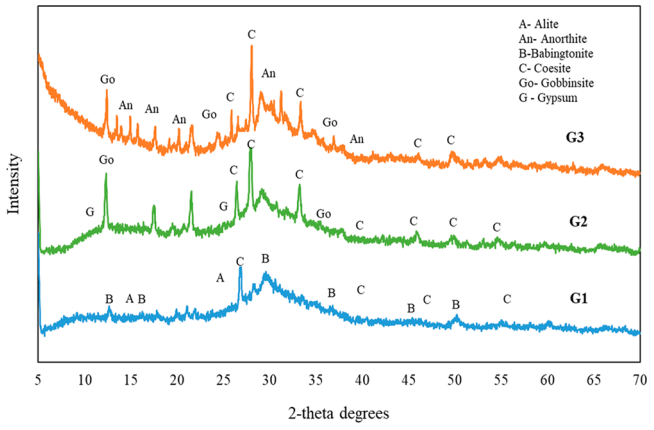

Figure 10. Diffractogram of geopolymer systems cured under different temperature conditions.

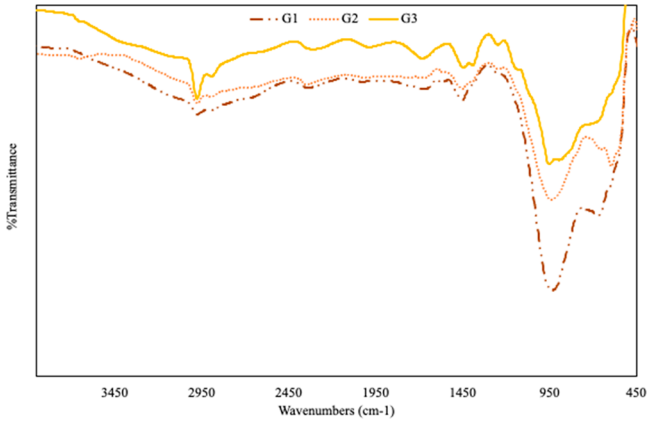

Figure 11. IR spectrum of geopolymer systems cured under different temperature conditions.

bonds due to the presence of new phases. The main band in Figure 11 occurs at 929−950 cm^{-1}, and it is a result of the asymmetric stretching of the Si−O−Si (Al) band of the geopolymer structure.[71] First of all, the shift of the asymmetric Si−O−Si (Al) peak to lower wavenumbers (1037 cm^{-1} to 929 cm^{-1} to 950 cm^{-1}) is an indication that geopolymerization has occurred, but the reduction in the intensity of the peak in this region with increasing curing temperature would suggest a breakdown of the gel structure.[72,73] This would be responsible

https://doi.org/10.1021/acsomega.1c06878
ACS Omega 2022, 7, 10268−10276

for the observed loss in strength reported by several authors for geopolymers subjected to higher curing temperatures.

3.5.3. TGA Geopolymer Systems. In general, the weight loss up to about 572 °F is because of the escape of physically and chemically bound water. The weight loss from 572 to 1202 °F is due to dehydration of the binding gel. In Figure 12, there is

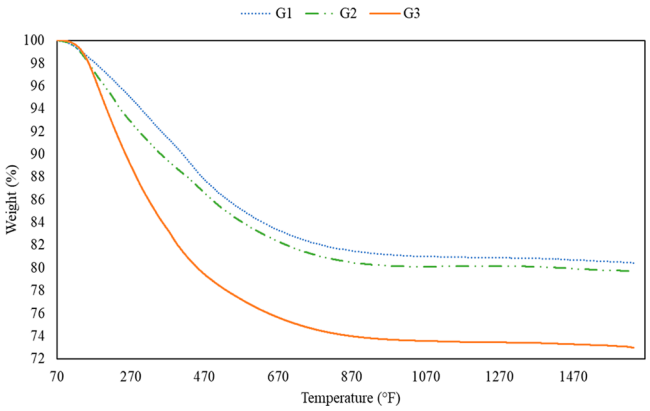

Figure 12. Thermogram of geopolymer systems cured under different temperature conditions.

greater weight loss in the geopolymer systems exposed to elevated temperatures. Higher weight loss would suggest the presence of a greater amount of cementitious gels. However, this is not the situation. It can be explained that at elevated temperatures, new phases are formed which would be unstable or could have more water molecules.[74,75] These factors would contribute to the higher mass loss in G2 and G3 geopolymer systems.

4. CONCLUSION

The application of geopolymer in oil-well cementing as an alternative to conventional Portland cement systems is currently being explored. This work focuses on the microstructural changes of geopolymer systems under elevated temperature conditions. The XRD, FTIR, and TGA techniques were used to observe this phenomenon. The findings indicate that when geopolymer is subjected to elevated temperatures, the gel structure is altered. This is due to the formation of crystalline phases. These phases may induce thermal stresses. This explains the reduction in the macroscopic properties of the geopolymer systems as reported by several authors.

AUTHOR INFORMATION

Corresponding Author

Salaheldin Elkatatny − *Department of Petroleum Engineering, College of Petroleum and Geosciences, King Fahd University of Petroleum and Minerals, Dhahran 31261, Saudi Arabia; Center for Integrative Petroleum Research, King Fahd University of Petroleum and Minerals, Dhahran 31261, Saudi Arabia;* orcid.org/0000-0002-7209-3715; Email: elkatatny@kfupm.edu.sa

Authors

Stephen Adjei − *Department of Petroleum Engineering, College of Petroleum and Geosciences, King Fahd University of Petroleum and Minerals, Dhahran 31261, Saudi Arabia; Department of Petroleum Engineering, Faculty of Civil and Geo-Engineering, Kwame Nkrumah University of Science and Technology, Kumasi 00000, Ghana*

Korhan Ayranci − *Department of Geosciences, King Fahd University of Petroleum and Minerals, Dhahran 31261, Saudi Arabia*

Complete contact information is available at: https://pubs.acs.org/10.1021/acsomega.1c06878

Notes

The authors declare no competing financial interest.

REFERENCES

(1) Worrell, E.; Price, L.; Martin, N.; Hendriks, C.; Meida, L. O. Carbon Dioxide Emissions from the Global Cement Industry. *Annu. Rev. Energy Environ.* **2001**, *26*, 303−329.

(2) Singh, N. B.; Middendorf, B. Geopolymers as an Alternative to Portland Cement: An Overview. *Constr. Build. Mater.* **2020**, *237*, 117455.

(3) Gartner, E. Industrially Interesting Approaches to "Low-CO2" Cements. *Cem. Concr. Res.* **2004**, *34* (9), 1489−1498.

(4) Davidovits, J. Mineral Polymers and Methods of Making Them. United States Patent. US4349386A, 1982.

(5) Davidovits, J. Geopolymers - Inorganic Polymeric New Materials. *J. Therm. Anal.* **1991**, *37* (8), 1633−1656.

(6) Adjei, S.; Elkatatny, S.; Aggrey, W. N.; Abdelraouf, Y. Geopolymer as the Future Oil-Well Cement: A Review. *J. Pet. Sci. Eng.* **2022**, *208*, 109485.

(7) Nasvi, M. C. M.; Ranjith, P. G.; Sanjayan, J. The Permeability of Geopolymer at Down-Hole Stress Conditions: Application for Carbon Dioxide Sequestration Wells. *Appl. Energy* **2013**, *102*, 1391−1398.

(8) Nasvi, M. C. M.; Ranjith, P. G.; Sanjayan, J. Effect of Different Mix Compositions on Apparent Carbon Dioxide (CO2) Permeability of Geopolymer: Suitability as Well Cement for CO2 Sequestration Wells. *Appl. Energy* **2014**, *114*, 939−948.

(9) Barlet-Gouedard, V.; Zusatz-Ayache, B.; Porcherie, O. Geopolymer Composition and Application for Carbon Dioxide Storage. US 7846250B2, 2010.

(10) Nasvi, M. C. M.; Rathnaweera, T. D.; Padmanabhan, E. Geopolymer as Well Cement and Its Mechanical Integrity Under Deep Down-Hole Stress Conditions: Application for Carbon Capture and Storage Wells. *Geomech. Geophys. Geo-Energy Geo-Resources* **2016**, *2* (4), 245−256.

(11) Lee, W. K. W.; Van Deventer, J. S. J. The Effects of Inorganic Salt Contamination on the Strength and Durability of Geopolymers. *Colloids Surfaces A Physicochem. Eng. Asp.* **2002**, *211* (2−3), 115−126.

(12) Nasvi, M. C. M.; Ranjith, P. G.; Sanjayan, J.; Haque, A.; Li, X. Mechanical Behaviour of Wellbore Materials Saturated in Brine Water with Different Salinity Levels. *Energy* **2014**, *66*, 239−249.

(13) Giasuddin, H. M.; Sanjayan, J. G.; Ranjith, P. G. Stress Versus Strain Behavior of Geopolymer Cement under Triaxial Stress Conditions in Saline and Normal Water. *Int. J. Civ. Environ. Eng.* **2013**, *7* (7), 521−524.

(14) Khalifeh, M.; Saasen, A.; Vrålstad, T.; Hodne, H. Potential Utilization of Geopolymers in Plug and Abandonment Operations. *Pap. Present. SPE Bergen One Day Semin.* Bergen, Norway, April. 2014, 389−402.

(15) Khalifeh, M.; Hodne, H.; Korsnes, R. I.; Saasen, A. Cap Rock Restoration in Plug and Abandonment Operations; Possible Utilization of Rock-Based Geopolymers for Permanent Zonal Isolation and Well Plugging. *Pap. Present. Int. Pet. Technol.*. Conf. Doha, Qatar, December 6−9. IPTC-18454-MS 2015. DOI: 10.2523/iptc-18454-ms.

(16) Salehi, S.; Ezeakacha, C. P.; Khattak, M. J. Geopolymer Cements: How Can. You Plug and Abandon a Well with New Class of Cheap Efficient Sealing Materials. *Pap. Present. SPE Oklahoma City Oil Gas Symp.*. Oklahoma City, Oklahoma, USA, March 27−31. SPE-185106-MS 2017. DOI: 10.2118/185106-ms.

(17) Rahman, S. H. B. A.; Irawan, S.; Shafiq, N.; Rajeswary, R. Investigating the Expansion Characteristics of Geopolymer Cement Samples in a Water Bath and Compared with the Expansion of ASTM Class-G Cement. *Heliyon* **2020**, *6* (2), No. e03478.

(18) Salehi, S.; Ali, N.; Khattak, M. J.; Rizvi, H. Geopolymer Composites as Efficient and Economical Plugging Materials in Peanuts Price Oil Market. *Pap. Present. SPE Annu. Tech*. Conf. Exhib. Dubai, UAE. Sept. 26−28. SPE-181426-MS 2016. DOI: 10.2118/181426-ms.
(19) Ahdaya, M.; Imqam, A. Investigating Geopolymer Cement Performance in Presence of Water Based Drilling Fluid. *J. Pet. Sci. Eng.* **2019**, *176*, 934−942.
(20) Olvera, R.; Panchmatia, P.; Juenger, M.; Aldin, M.; van Oort, E. Long-Term Oil Well Zonal Isolation Control Using Geopolymers: An Analysis of Shrinkage Behavior. *Pap. Present. SPE/IADC Int. Drill.* Conf. Exhib. Hague, Netherlands. March 5−7. SPE-194092-MS. 2019, 2019-March. DOI: 10.2118/194092-ms.
(21) Bu, Y.; Ma, R.; Du, J.; Guo, S.; Liu, H.; Zhao, L. Utilization of Metakaolin-Based Geopolymer as a Mud-Cake Solidification Agent to Enhance the Bonding Strength of Oil Well Cement-Formation Interface. *R. Soc. Open Sci.* **2020**, *7* (2). 191230.
(22) Eid, E.; Tranggono, H.; Khalifeh, M.; Salehi, S.; Saasen, A. Impact of Drilling Fluid Contamination on Performance of Rock-Based Geopolymers. *SPE J.* **2021**, *26*, 3626−3633.
(23) Nasvi, M. C. M.; Ranjith, P. G.; Sanjayan, J. *Comparison of Mechanical Behaviors of Geopolymer And Class G Cement as Well Cement at Different Curing Temperatures for Geological Sequestration of Carbon Dioxide*. Pap. Present. 46th U.S. Rock Mech. Symp. Chicago, Illinois. 24−27 June. ARMA-2012−232. 2012.
(24) Nasvi, M. C. M.; Gamage, R. P.; Jay, S. Geopolymer as Well Cement and the Variation of Its Mechanical Behavior with Curing Temperature. *Greenh. Gases Sci. Technol.* **2012**, *2* (1), 46−58.
(25) Nasvi, M. C. M.; Ranjith, P. G.; Sanjayan, J.; Bui, H. Effect of Temperature on Permeability of Geopolymer: A Primary Well Sealant for Carbon Capture and Storage Wells. *Fuel* **2014**, *117*, 354−363.
(26) Igbojekwe, S.; Salehi, S.; Khattak, M. J. Development of a New Geopolymer Based Cement: Laboratory Investigation. In *2015 AADE National Technical Conference and Exhibition*, San Antonio, Texas, April 8−9, **2015**. Paper NTCE-07.
(27) Ekaputri, J. J.; Priyanka, F. N. The Effect of Temperature Curing on Geopolymer Concrete. *MATEC Web Conf* **2017**, *97*, 01005.
(28) Al Bakria, A. M. M.; Kamarudin, H.; Bin Hussain, M.; Khairul Nizar, I.; Zarina, Y.; Rafiza, A. R. The Effect of Curing Temperature on Physical and Chemical Properties of Geopolymers. *Phys. Procedia* **2011**, *22*, 286−291.
(29) Ramalho, R. V. A.; Alves, S. M.; Freitas, J. C. D. O.; Costa, B. L. D. S.; Bezerra, U. T. Evaluation of Mechanical Properties of Cement Slurries Containing SBR Latex Subjected to High Temperatures. *J. Pet. Sci. Eng.* **2019**, *178*, 787−794.
(30) Albawi, A. *Influence of Thermal Cycling on Cement Sheath Integrity*; Institutt for petroleumsteknologi og anvendt geofysikk, 2013.
(31) Wu, J.; Wang, X.; Song, L.; Zhong, S.; Yin, W. Microannulus Formation Mechanism at the Cementing Interface of a Thermal Recovery Well during Cyclic Steam Injection. *Adv. Civ. Eng.* **2020**, *2020*, 1−11.
(32) Carroll, S.; Carey, J. W.; Dzombak, D.; Huerta, N. J.; Li, L.; Richard, T.; Um, W.; Walsh, S. D. C.; Zhang, L. Review: Role of Chemistry, Mechanics, and Transport on Well Integrity in CO2 Storage Environments. *Int. J. Greenh. Gas Control* **2016**, *49*, 149−160.
(33) Ostroot, G. W.; Walker, W. A. Improved Compositions for Cementing Wells with Extreme Temperatures. *J. Pet. Technol.* **1961**, *13* (03), 277−284.
(34) Bjørge, R.; Gawel, K.; Panduro, C. E. A.; Torsæter, M. Carbonation of Silica Cement at High-Temperature Well Conditions. *Int. J. Greenh. Gas Control* **2019**, *82*, 261−268.
(35) Nelson, E. B.; Guillot, D. *Well Cementing*, second ed; Schlumberger, 2006.
(36) Hunt, S. A.; Whitaker, M. L.; Bailey, E.; Mariani, E.; Stan, C. V.; Dobson, D. P. An Experimental Investigation of the Relative Strength of the Silica Polymorphs Quartz, Coesite, and Stishovite. *Geochemistry, Geophys. Geosystems* **2019**, *20* (4), 1975−1989.
(37) Alujas, A.; Fernández, R.; Quintana, R.; Scrivener, K. L.; Martirena, F. Pozzolanic Reactivity of Low Grade Kaolinitic Clays: Influence of Calcination Temperature and Impact of Calcination Products on OPC Hydration. *Appl. Clay Sci.* **2015**, *108*, 94−101.
(38) Ekosse, G. I. E. Fourier Transform Infrared Spectrophotometry and X-Ray Powder Diffractometry as Complementary Techniques in Characterizing Clay Size Fraction of Kaolin. *J. Appl. Sci. Environ. Manag.* **2005**, *9* (2), 43−48, DOI: 10.4314/jasem.v9i2.17289.
(39) Tironi, A.; Trezza, M. A.; Irassar, E. F.; Scian, A. N. Thermal Treatment of Kaolin: Effect on the Pozzolanic Activity. *Procedia Mater. Sci.* **2012**, *1*, 343−350.
(40) Adjei, S.; Elkatatny, S.; Ayranci, K.; Sarmah, P. Evaluation of Qusaiba Kaolinitic Shale as a Supplementary Cementitious Material in Lightweight Oil-Well Cement Formulation. Unpublisehed work, **2022**.
(41) Paiva, M. D. M.; Silva, E. C. C. M.; Melo, D. M. A.; Martinelli, A. E.; Schneider, J. F. A Geopolymer Cementing System for Oil Wells Subject to Steam Injection. *J. Pet. Sci. Eng.* **2018**, *169*, 748−759.
(42) Duxson, P.; Provis, J. L.; Lukey, G. C.; Mallicoat, S. W.; Kriven, W. M.; Van Deventer, J. S. J. Understanding the Relationship Between Geopolymer Composition, Microstructure and Mechanical Properties. *Colloids Surfaces A Physicochem. Eng. Asp.* **2005**, *269* (1−3), 47−58.
(43) Yip, C. K.; Lukey, G. C.; Provis, J. L.; van Deventer, J. S. J. Effect of Calcium Silicate Sources on Geopolymerisation. *Cem. Concr. Res.* **2008**, *38* (4), 554−564.
(44) Nath, P.; Sarker, P. K. Effect of GGBFS on Setting, Workability and Early Strength Properties of Fly Ash Geopolymer Concrete Cured in Ambient Condition. *Constr. Build. Mater.* **2014**, *66*, 163−171.
(45) Ionescu, B. A.; Lăzărescu, A. V.; Hegyi, A. The Possibility of Using Slag for the Production of Geopolymer Materials and Its Influence on Mechanical Performances—A Review. *Proceedings* **2020**, *63* (1), 30.
(46) *API RP 10B-2. Recommended Practice for Testing Well Cements*, 2nd ed.; American Petroleum Institute: New York, 2013.
(47) *API SPEC 10A. Specification for Cements and Materials for Well Cementing*, 23rd ed.; American Petroleum Institute: New York, 2002.
(48) Almenares, R. S.; Vizcaíno, L. M.; Damas, S.; Mathieu, A.; Alujas, A.; Martirena, F. Industrial Calcination of Kaolinitic Clays to Make Reactive Pozzolans. *Case Stud. Constr. Mater.* **2017**, *6*, 225−232.
(49) Konan, K. L.; Peyratout, C.; Smith, A.; Bonnet, J. P.; Rossignol, S.; Oyetola, S. Comparison of Surface Properties Between Kaolin and Metakaolin in Concentrated Lime Solutions. *J. Colloid Interface Sci.* **2009**, *339* (1), 103−109.
(50) Hicks, T. W.; White, M. J.; Hooker, P. J. *Role of Bentonite in Determination of Thermal Limits on Geological Disposal Facility Design*; Galson Sciences Ltd.: Oakham, England, 2010.
(51) Saikia, B. J.; Parthasarathy, G. Fourier Transform Infrared Spectroscopic Characterization of Kaolinite from Assam and Meghalaya, Northeastern India. *J. Mod. Phys.* **2010**, *01* (04), 206−210.
(52) Garcia-Valles, M.; Alfonso, P.; Martínez, S.; Roca, N. Mineralogical and Thermal Characterization of Kaolinitic Clays from Terra Alta (Catalonia, Spain). *Minerals* **2020**, *10* (2), 142.
(53) Zhao, Q.; Fu, L.; Jiang, D.; Ouyang, J.; Hu, Y.; Yang, H.; Xi, Y. Nanoclay-Modulated Oxygen Vacancies of Metal Oxide. *Commun. Chem.* **2019**, *2* (1), 1−10.
(54) Bayram, H.; Önal, M.; Yılmaz, H.; Sarıkaya, Y. Thermal Analysis of a White Calcium Bentonite. *J. Therm. Anal. Calorim.* **2010**, *101* (3), 873−879.
(55) Wang, H.; Wu, H.; Xing, Z.; Wang, R.; Dai, S. The Effect of Various Si/Al, Na/Al Molar Ratios and Free Water on Micro-morphology and Macro-Strength of Metakaolin-Based Geopolymer. *Materials (Basel)* **2021**, *14* (14), 3845.
(56) Duxson, P.; Fernández-Jiménez, A.; Provis, J. L.; Lukey, G. C.; Palomo, A.; Van Deventer, J. S. J. Geopolymer Technology: The Current State of the Art. *J. Mater. Sci.* **2007**, *42* (9), 2917−2933.
(57) Sisol, M.; Kudelas, D.; Marcin, M.; Holub, T.; Varga, P. Statistical Evaluation of Mechanical Properties of Slag Based Alkali-Activated Material. *Sustain.* **2019**, *11* (21), 5935.
(58) Ukritnukun, S.; Koshy, P.; Rawal, A.; Castel, A.; Sorrell, C. C. Predictive Model of Setting Times and Compressive Strengths for Low-Alkali, Ambient-Cured, Fly Ash/Slag-Based Geopolymers. *Minerals* **2020**, *10* (10), 920.

(59) Hattaf, R.; Aboulayt, A.; Samdi, A.; Lahlou, N.; Touhami, M. O.; Gomina, M.; Moussa, R. Reusing Geopolymer Waste from Matrices Based on Metakaolin or Fly Ash for the Manufacture of New Binder Geopolymeric Matrices. *Sustain* **2021**, *13* (14), 8070.
(60) Krizan, D.; Zivanovic, B. Effects of Dosage and Modulus of Water Glass on Early Hydration of Alkali−Slag Cements. *Cem. Concr. Res.* **2002**, *32* (8), 1181−1188.
(61) Choi, S.; Lee, K. M. Influence of Na2O Content and Ms (SiO2/Na2O) of Alkaline Activator on Workability and Setting of Alkali-Activated Slag Paste. *Materials (Basel)* **2019**, *12*, 2072.
(62) Cheng, H.; Lin, K. L.; Cui, R.; Hwang, C. L.; Chang, Y. M.; Cheng, T. W. The Effects of SiO2/Na2O Molar Ratio on the Characteristics of Alkali-Activated Waste Catalyst−Metakaolin Based Geopolymers. *Constr. Build. Mater.* **2015**, *95*, 710−720.
(63) Yip, C. K.; Lukey, G. C.; Van Deventer, J. S. J. The Coexistence of Geopolymeric Gel and Calcium Silicate Hydrate at the Early Stage of Alkaline Activation. *Cem. Concr. Res.* **2005**, *35* (9), 1688−1697.
(64) Zhang, Y. J.; Li, S.; Wang, Y. C.; Xu, D. L. Microstructural and Strength Evolutions of Geopolymer Composite Reinforced by Resin Exposed to Elevated Temperature. *J. Non. Cryst. Solids* **2012**, *358* (3), 620−624.
(65) Birch, W. D. *Babingtonite, Fluorapophyllite and Sphene from Harcourt*; Mineralogical Magazine: Victoria, Australia, 1982.
(66) Li, Z.; Ohnuki, T.; Ikeda, K. Development of Paper Sludge Ash-Based Geopolymer and Application to Treatment of Hazardous Water Contaminated with Radioisotopes. *Mater.* **2016**, *9* (8), 633.
(67) Karim, M. R. A.; Haq, E. U.; Hussain, M. A.; Khan, K. I.; Nadeem, M.; Atif, M.; Haq, A. U.; Naveed, M.; Alam, M. M. Experimental Evaluation of Sustainable Geopolymer Mortars Developed from Loam Natural Soil. *J. Asian Archit. Build. Eng.* **2020**, *19* (6), 637−646.
(68) Nikolov, A.; Rostovsky, I.; Nugteren, H. Geopolymer Materials Based on Natural Zeolite. *Case Stud. Constr. Mater.* **2017**, *6*, 198−205.
(69) Cheng-Yong, H.; Yun-Ming, L.; Abdullah, M. M. A. B.; Hussin, K. Thermal Resistance Variations of Fly Ash Geopolymers: Foaming Responses. *Sci. Reports* **2017**, *7* (1), 1−11.
(70) Ye, J.; Zhang, W.; Shi, D. Effect of Elevated Temperature on the Properties of Geopolymer Synthesized from Calcined Ore-Dressing Tailing of Bauxite and Ground-Granulated Blast Furnace Slag. *Constr. Build. Mater.* **2014**, *69*, 41−48.
(71) Petrus, H. T. B. M.; Olvianas, M.; Astuti, W.; Nurpratama, M. I. Valorization of Geothermal Silica and Natural Bentonite through Geopolymerization: A Characterization Study and Response Surface Design. *Int. J. Technol.* **2021**, *12* (1), 195−206.
(72) Khan, M. I.; Azizli, K. A.; Sufian, S.; Man, Z.; Khan, A. S.; Ullah, H.; Siyal, A. A. A Short Review of Infra-Red Spectroscopic Studies of Geopolymers. *Adv. Mater. Res.* **2016**, *1133*, 231.
(73) Ben Messaoud, I.; Hamdi, N.; Srasra, E. Physicochemical Characterization of Geopolymer Binders and Foams Made from Tunisian Clay. *Adv. Mater. Sci. Eng.* **2018**, *2018*, 1.
(74) Kumar, S.; Mucsi, G.; Kristály, F.; Pekker, P. Mechanical Activation of Fly Ash and Its Influence on Micro and Nano-Structural Behaviour of Resulting Geopolymers. *Adv. Powder Technol.* **2017**, *28* (3), 805−813.
(75) Kong, D. L. Y.; Sanjayan, J. G.; Sagoe-Crentsil, K. Comparative Performance of Geopolymers Made with Metakaolin and Fly Ash after Exposure to Elevated Temperatures. *Cem. Concr. Res.* **2007**, *37* (12), 1583−1589.

https://doi.org/10.1021/acsomega.1c06878
ACS Omega 2022, 7, 10268−10276